Quantum dynamics in a camel-back potential of a dc SQUID

Emile Hoskinson, Florent Lecocq, Nicolas Didier, Aurélien Fay, Frank. W. J. Hekking, Wiebke Guichard, Olivier Buisson, Ralf Dolata, Brigitte Mackrodt, Alexander B. Zorin

Quantum dynamics in a camel-back potential of a dc SQUID

E. Hoskinson[1], F. Lecocq[1], N. Didier[2], A. Fay[1], F. W. J. Hekking[2], W. Guichard[1] and O. Buisson[1]
[1]*Institut Néel, C.N.R.S.- Université Joseph Fourier, BP 166, 38042 Grenoble-cedex 9, France and*
[2]*LPMMC, C.N.R.S.- Université Joseph Fourier, BP 166, 38042 Grenoble-cedex 9, France*

R. Dolata, B. Mackrodt and A. B. Zorin
Physikalisch-Technische Bundesanstalt, Bundesallee 100, 38116 Braunschweig, Germany
(Dated: December 23, 2008)

We investigate a quadratic-quartic anharmonic oscillator formed by a potential well between two potential barriers. We realize this novel potential shape with a superconducting circuit comprised of a loop interrupted by two Josephson junctions (dc SQUID), with near-zero current bias and flux bias near half a flux quantum. We investigate escape out of the central well, which can occur via tunneling through either of the two barriers, and find good agreement with a generalized double-path macroscopic quantum tunneling theory. We also demonstrate that this system exhibits an "optimal line" in current and flux bias space along which the oscillator, which can be operated as a phase qubit, is insensitive to decoherence due to low-frequency current fluctuations.

PACS numbers: 85.25.Cp, 85.25.Dq, 03.67.Lx

Superconducting devices, based on the nonlinearity of the Josephson Junction (JJ), exhibit a wide variety quantum phenomena. During the last decade, inspired by Macroscopic Quantum Tunnelling (MQT) studies [1], quantum dynamics of the current biased JJ, dc SQUID and the rf SQUID phase qubit have been extensively studied [2–6]. In each of these devices, dynamics are analogous to those of a quantum particle in a quadratic-cubic potential. The flux qubit [7], realized by three or four JJs in a loop, is described by a double well potential.

We study a new potential shape called hereafter a "camel-back" double barrier potential, shown in Fig. 1c. This potential is obtained using the dc SQUID circuit shown in Fig. 1a in a new way. Characteristics including depth and relative barrier height are controlled by the SQUID current bias I_b and flux bias $\Phi_{\rm ext}$. There is an "optimal line" in the plane $(I_b, \Phi_{\rm ext})$ along which the barrier heights are equal and anharmonicity is quartic. We investigate the dynamics of the quantum system formed from the two lowest energy levels of the central well.

A dc SQUID circuit has two degrees of freedom corresponding to the phase differences ϕ_1 and ϕ_2 across its two JJs. Dynamics are analogous to those of a particle of mass $m = 2C(\Phi_0/2\pi)^2$ in the 2-D potential [8, 9]

$$U(x,y) = U_0[-\cos x\cos y - sx + b\,(y-y_b)^2 - \alpha\sin x\sin y - \eta s y]. \quad (1)$$

Here $x = (\phi_1+\phi_2)/2, y = (\phi_1-\phi_2)/2$, $U_0 = (I_{c1}+I_{c2})\Phi_0/2\pi$, $b = \Phi_0/\pi L I_c$ is the junction to loop inductance ratio, $\alpha = (I_{c2}-I_{c1})/I_c$ is the critical current asymmetry, $\eta = (L_2-L_1)/L$ is the loop inductance asymmetry, $I_c = I_{c1}+I_{c2}$, I_{c1} and I_{c2} are the critical currents of the two junctions, L_1 and L_2 are the geometric inductances of the two arms of the SQUID loop, $L = L_1+L_2$, C is the capacitance of each junction, and $\Phi_0 = h/2e$ is the quantum of flux. The external control parameters I_b and $\Phi_{\rm ext}$ enter through $y_b = \pi\Phi_{\rm ext}/\Phi_0$ and $s = I_b/I_c$. For our sample, $I_c = 11.22$ μA, $C = 250.3$ fF, $b = 3.05$, $\eta = 0.72$, and $\alpha = 0.0072$.

Stable, stationary states of the system correspond to minima of $U(x,y)$. There can exist one or more minima families corresponding to distinct fluxoid states $[n\Phi_0]$. For each, when s exceeds a flux dependent critical value $s_c[n\Phi_0](y_b)$, the related local minima disappear. For small values of b, the parabolic term in $U(x,y)$ is shallow, and there can be many fluxoid states. For $b \gg 1/\pi$, as in our case, the parabolic term is steep and there is only one stable fluxoid state except in a small region around $\Phi_{\rm ext}/\Phi_0 \approx 0.5(\text{mod } 1)$ where there are two states with opposite circulating currents. Hereafter we will be focusing on this region.

In general, dynamics is described by 2-D motion in the potential. In our device, motion is well approximated as 1-D along the minimum energy path which connects minima and saddle points (black line in Fig. 1b). A large curvature in the orthogonal direction confines the system to this path. For example, at the $[0\Phi_0]$ minima in Fig. 1b, the oscillation frequency along the path is $\omega_{px} \equiv \sqrt{(\partial^2 U/\partial x^2)/m} = 2\pi \times 15.4$ GHz, whereas $\omega_{py} = 2\pi \times 104$ GHz. We parametrize the path with the phase length z. $U(z)$ in Fig. 1c depicts the "camel-back" potential shape we are investigating. In a typical experiment, the system is initialized in the central well ($[0\Phi_0]$ state). The system can escape via tunneling through the barriers in either of the two physically distinct directions to the [-1Φ_0] state.

In the symmetric case, the potential near the central minimum will be harmonic with a quartic perturbation. More generally, the Hamiltonian for small oscillations in $U(z)$ is $\hat{H} = \hbar\omega_p(\hat{P}^2+\hat{Z}^2)/2 - \sigma\hbar\omega_p\hat{Z}^3 - \delta\hbar\omega_p\hat{Z}^4$. Here ω_p is the zero amplitude oscillation frequency in the direction of minimum curvature, and $\hat{Z} = z\sqrt{m\omega_p/\hbar}$ and $\hat{P} =$

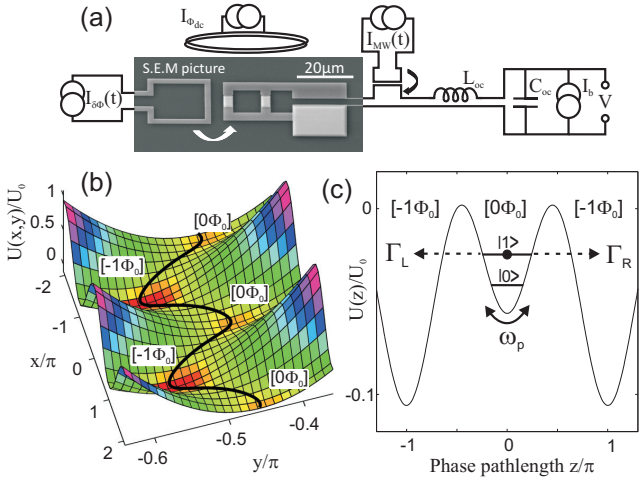

FIG. 1: Experimental setup. (a) Circuit layout. The two small white squares in the central loop are the SQUID JJs. Connected on the right are current bias and voltage leads. These are heavily filtered at various stages of the cryostat, including the on-chip low-pass filter formed by $L_{\rm oc} = 10$ nH and $C_{\rm oc} = 200$ pF [10]. Fast flux pulses $\delta\Phi$ inductively couple via the on-chip loop to the left of the SQUID. Microwave excitation is applied via an on-chip loop which couples inductively to the current bias leads [11]. An off-chip coil provides a dc flux bias $\Phi_{\rm dc}$. The total externally applied flux is $\Phi_{\rm ext} = \Phi_{\rm dc} + \delta\Phi$. The SQUID chip is enclosed in a copper box thermally anchored to the mixing chamber of a dilution refrigerator with a 30 mK base temperature. The cryostat is surrounded by superconducting Pb, μ-metal, and soft iron shielding. (b) Full 2-D potential for $b = 3.05$, $\eta = 0.72$, $\alpha = 0$, $\Phi_{\rm ext} = -0.508\Phi_0$, $I_b = 0$, showing the families of minima associated with the $[0\Phi_0]$ and $[-1\Phi_0]$ fluxoid states. The black line follows the minimum energy path. Note the difference in the x and y scales. (c) Potential along the minimum energy path, parameterized by the path length.

$p/\sqrt{\hbar\omega_p m}$ are the reduced position and corresponding momentum operators. Treating the anharmonic terms as perturbations, to second order the transition energy between levels $n-1$ and n is $h\nu_{n-1,n} = \hbar\omega_p(1 - n\Lambda)$, where the anharmonicity is $\Lambda = \frac{15}{2}\sigma^2 + 3\delta$ [12].

We have calculated the escape probability for the camel-back potential with a double escape path in the quantum limit using the instanton formalism [13]. For a duration Δt, it reads $P_{\rm esc}(I_b, \Phi_{\rm ext}) = 1 - {\rm e}^{-(\Gamma_R+\Gamma_L)\Delta t}$, where $\Gamma_{R,L} = A_{R,L}\omega_p\sqrt{N_{R,L}}\,\exp[-B_{R,L}N_{R,L}]$. Here R and L refer to the right and left barriers. $N_{R,L} = \Delta U_{R,L}/\hbar\omega_p$ are the normalized barrier heights. The general expressions for $A_{R,L}$, and $B_{R,L}$ depend on the potential shape. In the symmetric case where $\sigma(I_b, \Phi_{\rm ext}) = 0$, the potential is quadratic-quartic, $A_{R,L} = 2^{\frac{5}{2}}\pi^{-\frac{1}{2}}$ and $B_{R,L} = 16/3$. Far from this symmetric line the potential is quadratic-cubic, the escape rate through one barrier is dominant (*e.g.* $\Gamma_L = 0$), and we retrieve the standard MQT situation ($\delta = 0$): $A_R = 6^{\frac{3}{2}}\pi^{-\frac{1}{2}}$ and $B_R = 36/5$ [1].

A schematic of our experimental setup is shown in Fig. 1a. Our sample was fabricated at Physikalisch-Technische Bundesanstalt using a Nb/AlO_x/Nb trilayer process with SiO_2 dielectric [14]. The two 5 μm^2 junctions are embedded in a 10x10 μm^2 square loop.

Fig. 2a shows the escape lines, $I_{50\%}$ versus $\Phi_{\rm ext}$. This data was obtained with a standard technique in which I_b pulses of varying amplitude are applied and a dc voltage detected across the SQUID when it switches to its voltage state. With this scheme there is no direct indication of multiply stable flux states. In Fig. 2b we use a novel technique to measure the overlapping escape lines of $[0\Phi_0]$ and $[-1\Phi_0]$ flux states close to $\Phi_{\rm ext}/\Phi_0 = -0.5$. For $|I_b|$ less than about 0.5 μA, these two interior escape lines represent transitions between the two flux states, rather than transitions to the voltage state.

We illustrate our escape measurement method by describing a sequence used to measure $P_{\rm esc}$ at a point, noted M, near the left cusp of Fig. 2b. The sequence starts at point S, with current bias I_b and $\Phi_{\rm ext} = \Phi_{\rm dc}$. Here the system is initialized in the $[0\Phi_0]$ fluxoid state, if necessary with an adiabatic pulse on the fast flux line. A flux pulse $\delta\Phi$ is then applied via the fast line for a fixed nanosecond-scale duration, bringing the total externally applied flux $\Phi_{\rm ext} = \Phi_{\rm dc} + \delta\Phi$ to point M close to the critical line. This has the effect of reducing the heights $\Delta U_{R,L}$ of the two potential barriers, greatly enhancing $P_{\rm esc}$, and the system may escape to the $[-1\Phi_0]$ fluxoid state. $\Phi_{\rm ext}$ drops back to $\Phi_{\rm dc}$ (point S), where both fluxoid states are stable. The fluxoid state is then read out via a slow (~ 10 μs) I_b pulse which brings the system to point R outside the critical line of fluxoid state $[-1\Phi_0]$ but well within that of $[0\Phi_0]$. If the system is in state $[-1\Phi_0]$, the SQUID will switch, producing a voltage which is detected [15]. If it is in state $[0\Phi_0]$, it will not switch. We achieve a one-shot discrimination between flux states of 100% with this readout. The process is completed by bringing I_b to zero for 100 μs where retrapping occurs and heat generated by a switching event dissipates. Multiple repetitions, at a rate of about 5 kHz, yield $P_{\rm esc}$ at point M. By varying points S, M, R, and the initial fluxoid state, we are able to measure $P_{\rm esc}$ for each of the two fluxoid states at any $(I_b, \Phi_{\rm ext})$ point in this region. For $|I_b| > 0.5$ μA, the system escapes directly to the voltage state at point M, rendering point R unnecessary.

As shown by the fit in Fig. 2b, our generalized MQT theory is accurately able to reproduce the data. Of the parameters that go into this theory, b and α are treated as free parameters in this fit, I_c, η, and the $\Phi_{\rm dc}$ calibration are determined by the fit in Fig. 2a, the fast flux pulse calibration is determined by matching $P_{\rm esc}(\Phi_{\rm ext})$ curves obtained with different values of $\Phi_{\rm dc}$, and C is determined by a fit to spectroscopic data.

Along the escape line of a given fluxoid state, for I_b above or below the value $I_b^{\rm cusp}$, the potential (Fig. 1c) is tilted to the right or to the left, and escape occurs preferentially in that direction. At $I_b^{\rm cusp}$, the camel potential

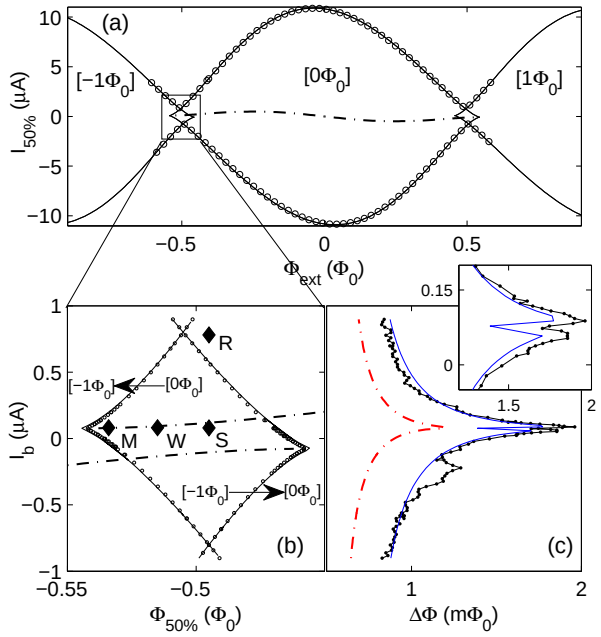

FIG. 2: Ground-state escape. (a) Escape lines of three fluxoid states as measured by $I_{50\%}$, the amplitude of a 60 μs I_b pulse that yields $P_{\rm esc} = 50\%$ to the voltage state of the SQUID. Data (symbols), and standard MQT theory fit (solid lines). Here $\delta\Phi = 0, \Phi_{\rm ext} = \Phi_{\rm dc}$. The calculated $I_b^{\rm op}(\Phi_{\rm ext})$ for the $[0\Phi_0]$ state is indicated by the dash-dot line. (b) Overlapping escape lines in the region $\Phi_{\rm ext} \simeq -\Phi_0/2$. Data (symbols), and generalized MQT theory fit (solid lines), as measured by $\Phi_{50\%}$, where $\Phi_{\chi\%}$ is the total applied flux $\Phi_{\rm ext} = \Phi_{dc} + \delta\Phi$ that yields $P_{\rm esc} = \chi\%$ from the $[-1\Phi_0]$ to the $[0\Phi_0]$ state (right cusp) or vice-versa (left cusp). $\delta\Phi$ is the amplitude of a 100 ns flux pulse. For $|I_b|$ above about 0.5 μA, escape occurs directly to the voltage state of the SQUID. The cusps occur at a non-zero current bias $I_b^{\rm cusp} \simeq \pm\alpha I_c = \pm 81$ nA due to the critical current asymmetry α. The horizontal separation of the cusps scales precisely with $1/b$. The uppper (lower) dash-dot line indicates the calculated $I_b^{\rm op}(\Phi_{\rm ext})$ for the $[0\Phi_0]$ ($[-1\Phi_0]$) state. The points S, W, M, and R indicate the Starting, Working, quantum Measurement, and Readout points for a typical camel-back phase qubit experiment. (c) Width of ground-state escape $\Delta\Phi = |\Phi_{80\%} - \Phi_{20\%}|$, measurements (points+lines), and generalized MQT theory with (solid line) and without (dash-dot line) 9 nA RMS low-frequency current noise. The location of the dip near the maximum $\Delta\Phi$ corresponds to the point where symmetry leads to a reduction in sensitivity to noise.

is symmetric around the minimum ($\sigma = 0$), the two potential barrier heights are equal, and escape occurs with equal probability in either direction. The cusps in Fig. 2b correspond therefore to a double-path escape.

The width of the escape process contains additional information about the dependence of the potential on the bias parameters, and on fluctuations in the bias parameters [16]. In Fig. 2c, we plot the width as a function of I_b. This plot peaks around $I_b^{\rm cusp}$, except that at this point there is a sharp dip (see inset). This behavior is explained by double-path MQT if we include low frequency current fluctuations. In this circuit thermal fluctuations are expected in I_b, which we estimate to be on the order of 10 nA RMS by the equipartition theorem $\frac{1}{2}kT = \frac{1}{2}L_{\rm oc}I_{\rm RMS}^2$, where k is Boltzmann's constant, $T \simeq 40$ mK is the circuit temperature, and $L_{\rm oc} = 10$ nH is the series isolating inductance. Because of this noise, $P_{\rm esc}(I_b, \Phi_{\rm ext})$ is convolved with the probability distribution of I_b, which we assume to be Gaussian with standard deviation $I_{\rm RMS}$. As shown in Fig. 2c, $I_{\rm RMS} = 9$ nA is accurately able to explain both the increase in the overall width, and the presence of a distinctive dip at $I_b^{\rm cusp}$, a result of symmetry in escape direction. The presence of the dip and our ability to reproduce it with MQT theory is a striking confirmation of double path escape and low frequency I_b fluctuations in our sample.

In Fig. 3 we investigate the operation of a phase qubit composed of the $|0\rangle$ and $|1\rangle$ levels of the anharmonic central well of the camel-back potential. We use the same procedure as for the ground-state escape measurements, except $\delta\Phi$ is split into two steps. The first takes the system from point S to W, where the qubit is manipulated by microwave (MW) pulses applied to the fast current line. The system is then taken to point M for 5 ns, which projects the qubit state onto the flux state of the SQUID. This is possible because $P_{\rm esc}$ depends exponentially on the excitation level of the qubit. This flux coordinate of M is tuned such that escape will occur with high probability if the qubit is excited, and low probability if it is not. This measurement step thus projects the quantum states $|0\rangle$ and $|1\rangle$ of the qubit to the classical fluxoid states $[0\Phi_0]$ and $[-1\Phi_0]$ of the SQUID, which are stable at point S. Readout of the fluxoid state at point R reveals the projected qubit state. Repetition yields $P_{\rm esc}$, giving the probability of finding the qubit in its excited state with a contrast of about 50%.

$P_{\rm esc}$ was measured as a function of I_b and the frequency ν of a single 800 ns duration MW pulse applied to the qubit. Because the duration is much longer that the relaxation time $T_1 \simeq 100$ ns, the qubit reaches a steady state. $P_{\rm esc}$ is enhanced when ν matches the qubit transition frequency ν_{01} (Fig. 3a). The maximum in ν_{01} occurs at $I_b^{\rm op}(\Phi_{\rm ext})$, which corresponds to the camel potential symmetric point. Note that this optimal line (see Fig 2b) is a function of flux, and is terminated by the cusp at the critical line. Apparent in this spectroscopic image are avoided level crossings with what are likely microscopic two-level fluctuators, as first observed by Ref. [3]. We observe on average 20 crossings per GHz. In Fig. 3b, the spectroscopic width $\Delta\nu_{01}$ of the ν_{01} transition , obtained from Fig. 3a, is plotted as a function of I_b. A sharp minimum is observed at $I_b = 108$ nA, corresponding to the flat maximum in ν_{01}.

We find that we can accurately model $\Delta\nu_{01}(I_b)$ with a combination of low-frequency current and flux fluctuations. Because ν_{01} depends on the bias parameters, fluc-

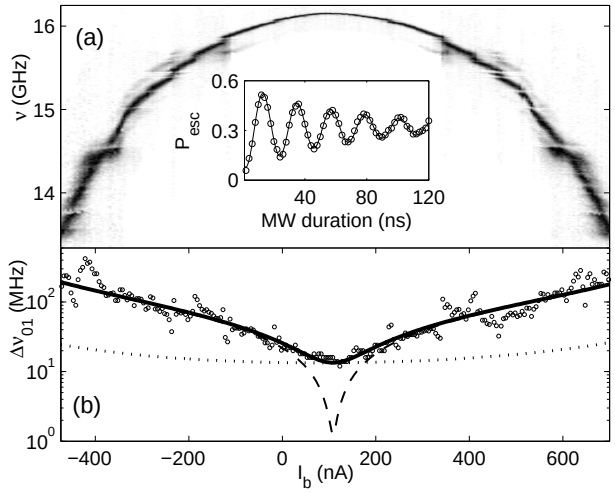

FIG. 3: Camel-back potential phase qubit. (a) Spectroscopy $P_{\rm esc}(I_b,\nu)$ at $\Phi_{\rm ext} = -0.503\Phi_0$ in the $[0\Phi_0]$ fluxoid state. Dark and bright grayscale correspond to high and small $P_{\rm esc}$. $P_{\rm esc}$ is enhanced when ν matches ν_{01}. Inset: Rabi oscillations on the optimal line. (b) Width of the ν_{01} resonance on a semi-log scale. The dashed line is the predicted contribution due to 9 nA RMS low-frequency current noise. The dotted line is for 40 $\mu\Phi_0$ RMS low-frequency flux noise. The sum of these two contributions, the solid line, accurately reproduces the data (symbols).

tuations cause ν_{01} to vary from repetition to repetition, smearing out the observed resonance. Assuming a Gaussian fluctuation distribution, the predicted variance in ν_{01} is $(\Delta\nu_I/2)^2 = (\partial_{I_b}\nu)^2 I_{\rm RMS}^2 + (\partial_{I_b}^2\nu)^2 I_{\rm RMS}^4/2$, for current fluctuations alone, and $(\Delta\nu_\Phi/2)^2 = (\partial_{\Phi_{\rm ext}}\nu)^2\Phi_{\rm RMS}^2$ for flux fluctuations alone. Here $\partial_x\nu \equiv \partial\nu_{01}/\partial x$. $\Delta\nu_I$ has been expanded to second order in $I_{\rm RMS}$ since $\partial_{I_b}\nu$ is zero at the optimal line. In Fig. 3b, the predicted $\Delta\nu_I$ is plotted as a dashed line for $I_{\rm RMS} = 9$ nA, precisely the same current fluctuation amplitude used in Fig. 2c. The dotted line plots $\Delta\nu_\Phi$ for $\Phi_{\rm RMS} = 40\ \mu\Phi_0$. The solid line is the combined prediction $\Delta\nu = \sqrt{\Delta\nu_I^2 + \Delta\nu_\Phi^2}$. The dashed line is obscured behind the solid line except in a small region around the optimal current. This plot vividly demonstrates the idea of the optimal line: the effects of current bias fluctuations, which accurately account for the spectral width away from the optimal line, are rendered negligible on the optimal line. The residual spectroscopic width, about 15 MHz, can be explained by a flux noise of 40 $\mu\Phi_0$ RMS.

Since the decoherence time T_2 scales inversely with $\Delta\nu_{01}$, $I_b^{\rm op}(\Phi_{\rm ext})$ is optimal for qubit operations. We measured Rabi oscillations on this line by varying the duration of a resonant MW excitation pulse, as shown in the inset to Fig. 3a. We find a typical Rabi decay time of $T_{\rm Rabi} = 67$ ns for this sample. The anharmonicity is large enough and the applied power small enough that excitation beyond the first excited state is negligible, as we have verified by the linearity of Rabi frequency versus power. The system is confined to its lowest two levels and can therefore be considered a qubit.

In conclusion, we have studied the quantum dynamics of a novel quadratic-quartic "camel" potential created in a dc SQUID circuit with $I_b \simeq 0$, $\Phi_{\rm ext} \simeq 0.5\Phi_0$. Ground-state escape exhibits critical line cusps and a dip in the escape width versus bias-current. We explain these two effects with a generalized double-path MQT escape theory. Moreover due to the particular potential symmetry, the quantum dynamics is insensitive in first order to current fluctuations along an optimal line $I_b^{\rm op}(\Phi_{\rm ext})$. Along this line, the dc SQUID can be used as a phase qubit whose main decoherence source is residual flux noise. Future optimization and exploitation of the unique properties of this system will aid in the understanding of decoherence mechanisms in quantum circuits and has the potential to yield a competitive phase qubit.

This work was supported by two ACI programs, by the EuroSQIP and INTAS projects.

[1] *Quantum Tunneling in Condensed Media*, Modern Problems in Condensed Matter Sciences, Vol. 34, edited by Yu. Kagan and A. J. Leggett (Elsevier Science Publishers, 1992).
[2] J. M. Martinis, S. Nam, J. Aumentado, and C. Urbina, Phys. Rev. Lett. **89**, 117901 (2002).
[3] K.B. Cooper *et al.*, Phys. Rev. Lett. **93**, 180401 (2004).
[4] J. Claudon, F. Balestro, F. W. J. Hekking, and O. Buisson, Phys. Rev. Lett. **93**, 187003 (2004).
[5] J. Lisenfeld, A. Lukashenko, M. Ansmann, J. M. Martinis, and A. V. Ustinov, Phys. Rev. Lett **99**, 170504 (2007).
[6] S. K. Dutta *et al.*, arXiv 0806.4711 (2008).
[7] I. Chiorescu, Y. Nakamura, C. J. P. M. Harmans, and J. E. Mooij, Science **299**, 1869 (2003).
[8] C. D. Tesche and J. Clarke, J. Low Temp. Phys. **29**, 301 (1977).
[9] V. Lefevre-Seguin, E. Turlot, C. Urbina, D. Esteve, and M. H. Devoret, Phys. Rev. B **46**, 5507 (1992).
[10] A. Fay, PhD thesis, Université Joseph Fourier, 2008.
[11] The MW excitation must be in *current*, rather than flux, because for the symmetric camel potential, small amplitude oscillations occur mainly in the x direction, and therefore are excited via the $-sx$ term in $U(x,y)$.
[12] L. D. Landau and L. M. Lifshitz, *Quantum Mechanics: Non-Relativistic Theory* (Course of Theoretical Physics, Volume 3), (3ed., Pergamon, 1991).
[13] C. G. Callan and S. Coleman, Phys. Rev. D **16**, 1762 (1977).
[14] R. Dolata, H. Scherer, A. B. Zorin, and J. Niemeyer, J. Appl. Phys. **97**, 054501 (2005).
[15] The flux coordinate of point R, equal to $\Phi_{\rm dc}$, must be chosen to be close to the intersection of the $[-1\Phi_0]$ and $[0\Phi_0]$ critical lines, where the $[0\Phi_0]$ well is relatively shallow. This ensures that SQUID voltage switching can be achieved, as opposed to retrapping in the $[0\Phi_0]$ well.
[16] J. Claudon, A. Fay, E. Hoskinson, and O. Buisson, Phys. Rev. B **76**, 024508 (2007).